^{129}Xe Nuclear Magnetic Resonance Study of Pitch-Based Activated Carbon Modified by Air Oxidation/Pyrolysis Cycles: A New Approach to Probe the Micropore Size

Konstantin V. Romanenko,*,†,‡ Xavier Py,§ Jean-Baptiste d'Espinose de Lacaillerie,‡,|| Olga B. Lapina,† and Jacques Fraissard‡

Boreskov Institute of Catalysis, Siberian Branch of Russian Academy of Sciences, Novosibirsk, 630090 Russia, CNRS-PROMES, Processes Materials and Solar Energy Laboratory, Rambla de la Thermodynamique, Tecnosud, 66100 Perpignan Cedex, France, and Laboratoire de Physique Quantique and UMR CNRS 7142, Ecole Supérieure de Physique et de Chimie Industrielles (ESPCI), 75231 Paris Cedex 05, France

Received: September 8, 2005; In Final Form: December 16, 2005

^{129}Xe NMR has been used to study a series of homologous activated carbons obtained from a KOH-activated pitch-based carbon molecular sieve modified by air oxidation/pyrolysis cycles. A clear correlation between the pore size of microporous carbons and the ^{129}Xe NMR of adsorbed xenon is proposed for the first time. The virial coefficient δ_{Xe-Xe} arising from binary xenon collisions varied linearly with the micropore size and appeared to be a better probe of the microporosity than the chemical shift extrapolated to zero pressure. This correlation was explained by the fact that the xenon collision frequency increases with increasing micropore size. The chemical shift has been shown to vary very little with temperature (less than 9 ppm) for xenon trapped inside narrow and wide micropores. This is indicative of a smooth xenon−surface interaction potential.

1. Introduction

The suitability of carbon materials in catalysis as well as in other strategic applications is related to some important surface properties of these materials (surface area, porosity, chemical inertness, and the occurrence of surface oxygen groups). Besides the ordinary adsorption techniques, the use of ^{129}Xe NMR is generally accepted for characterization of zeolites and mesoporous and amorphous silica. In contrast, ^{129}Xe NMR has been only rarely used to study carbon materials.

Partially due to the dispersion of structural/surface properties, paramagnetism, and different impurities, activated carbons are among the most complicated materials. From this point of view, original approaches such as ^{129}Xe NMR are extremely important. Not many studies on ^{129}Xe NMR as a probe of porous carbon texture have been published,[1−11] and few of them aimed at finding ^{129}Xe NMR correlations with various textural properties. Using amorphous carbons of different nature (precursor origin, preparation method, and surface chemistry) to obtain a set of samples of different pore sizes is a major drawback in these studies. In our work, this was overcome by using a new pore size tailoring technique.[12] A series of activated carbons was obtained by successive air oxidation/pyrolysis cyclic treatments of a unique precursor, leading to a gradual increase in the micropore size by 1.8 Å steps.

Successive widening cycles consist of an initial molecular oxygen sorption step, followed by a carbonization step under nitrogen. During the first step, oxygen is uniformly chemisorbed at the available intraparticular surface of the material. All carbon atoms available at the edge of the adsorbent graphene layers are oxidized uniformly without combustion. During the second step, the obtained oxygen-containing groups are withdrawn with the corresponding carbon atoms, leading to a reduction in graphene layer size and consequently to an increase in the mean pore size. In this way, preferential initiation of new micropores takes place and preferential burnoff at the pore mouth is avoided.

Compared to the conventional activation procedure, this method allows avoidance of the usual competition between activating agent diffusion and reaction within the particle which is often responsible for radial heterogeneity in textural pore parameters. Therefore, the series of modified activated carbons obtained presents narrow pore size distributions of particular interest for carbon molecular sieve (CMS) applications. The samples conserve the same basic carbonaceous structure and surface chemistry.

Similarly to the results obtained for xenon gas,[13,14] the variation of the isotropic chemical shift against the density (ρ) of xenon adsorbed in zeolites is given by:[15]

$$\delta(T, \rho) = \delta_S(T) + \delta_{Xe-Xe}(T)\rho + \delta_{Xe-Xe-Xe}(T)\rho^2 + ... \quad (1)$$

The virial coefficients δ_S, $\delta_{Xe-Xe,}$ and $\delta_{Xe-Xe-Xe}$ are temperature-dependent.[16] For the pure materials, δ_S is regarded as a surface characteristic dependent on the Xe diffusion rate. In the initial studies,[17,18] δ_S was correlated with the mean free path of xenon $\bar{l}$ imposed by the micropore structure of zeolites and molecular sieves. In the case of zeolites, the empirical equation is given as

$$\delta_S = 243\frac{0.2054}{0.2054 + \bar{l}} \quad (2)$$

The term $\delta_{Xe-Xe}\rho$ arises from binary collisions of xenon atoms in a confined space and depends on the pore size and shape. It

* Corresponding author: tel. 007 3832 3397267; fax 007 3833 3308056; E-mail address kostaromavita@ngs.ru.

† Siberian Branch of Russian Academy of Sciences.

‡ Laboratoire de Physique Quantique, Ecole Supérieure de Physique et de Chimie Industrielles (ESPCI).

§ CNRS-PROMES, Processes Materials and Solar Energy Laboratory.

|| UMR CNRS 7142, Ecole Supérieure de Physique et de Chimie Industrielles (ESPCI).

10.1021/jp055064g CCC: $33.50
Published on Web 01/31/2006

may be considered to be an additional probe of the material studied. The term $\delta_{Xe-Xe-Xe}\rho^2$ is significant only at very high xenon density ($\gg$10 mmol·cm^{-3}).

First attempts to analyze experimental δ_{Xe-Xe} values with respect to the porosity look promising. In the work of Julbe et al.,[19] the slope δ_{Xe-Xe} was correlated with the pore size of a sol−gel derived amorphous microporous silica. The authors concluded that δ_{Xe-Xe} decreases with increasing pore size. However, the slope values of δ_{Xe-Xe} were obtained from the chemical shift as a function of xenon pressure (P_{Xe}). The conclusions so obtained are questionable since the xenon density does not vary linearly with Xe pressure in the full pressure range. This is particularly true in micropores. Nevertheless, on the basis of numerical calculations, the authors emphasized that the term $\delta_{Xe-Xe}(D)$ is a better probe of the micropore size than δ_S.

A result qualitatively different from the previous one was obtained by Chen et al.[20] A new approach to calculate the size of narrow one-dimensional channels is based on the confined one-dimensional collision model. According to this approach, the channel diameter D (nm) is related to δ_{Xe-Xe} (ppm·amagat^{-1}) as

$$D = 1.681\delta_{Xe-Xe}^{1/2} \quad (3a)$$

Or using δ_{Xe-Xe} in ppm·cm^3·mmol^{-1} (1 amagat is equal to 0.045 mmol/cm^3):

$$D = 0.356\delta_{Xe-Xe}^{1/2} \quad (3b)$$

In this model, the slope δ_{Xe-Xe} is then an increasing function of the pore size. This dependence is related to single-file diffusion (SFD) phenomenon.[21−25] For molecules in a channel with a diameter less than twice the molecular size, the diffusion character is different from that of diffusion in much wider pores. As δ_{Xe-Xe} is proportional to the xenon collision frequency (ν), in a one-dimensional channel, it increases with increasing collision cross-sectional area (σ): $\delta_{Xe-Xe} \sim \nu \sim \sigma \sim D^2$.

Equation 3a was tested on the experimental data published earlier for various microporous zeolites. The pore diameters were calculated using experimental δ_{Xe-Xe} values and compared to the channel characteristics measured by X-ray diffraction (XRD). In most cases, this equation provides a better estimate of the pore size than eq 2, if it is assumed that the pore size calculated from XRD is very precise. Indeed, the latter depends on the choice of the encumbering of the oxygen atom at the surface. For a Y zeolite, eq 3 gave the pore size with a relatively large error (∼0.3 nm), which is not surprising, since the distribution of Xe−Xe collisions in the zeolite supercages is assumed to be isotropic.

In a study of microporous amorphous carbons of various origins,[4] the close values of δ_{Xe-Xe} were ascribed to two-dimensional Xe−Xe collisions on the surface of slitlike pores. The frequency of Xe−Xe collisions in the volume was neglected. However, since micropore filling is not described by the simple mono- or multilayer adsorption models and the volume influence is not negligible, the above interpretation remains questionable.

Here, we demonstrate the potential of ^{129}Xe NMR for microporous amorphous carbon characterization with a particular emphasis on the analysis of the δ_{Xe-Xe} to that effect.

2. Experimental Section

A series of activated carbons was synthesized by successive cyclic air oxidation/pyrolysis treatments of the same precursor as described in ref 12. The initial activated carbon was a laboratory-made carbon molecular sieve (CMS) obtained by activation of a maturated coal tar pitch precursor by mild oxidation by KOH with a pitch/KOH weight ratio of 1:0.5. Each activated carbon from the modified CMS series was obtained by sampling 1 g of an initial CMS load of 20 g after each successive pore size widening treatment. The oxidation step was performed in air at 473 K for 8 h; the following pyrolysis step was performed in nitrogen at 1173 K for 2 h.

TABLE 1: Textural Properties of the Series of Activated Carbons[a]

cycle	D (nm)	W_t (cm^3·g^{-1})	W_0 (cm^3·g^{-1})	S_{BET} (m^2·g^{-1})	S_{EXT} (m^2·g^{-1})
1	0.67	0.35	0.33	846	
2	0.84	0.5	0.44	1157	8.00
3	0.97	0.48	0.42	1104	8.30
4	1.1	0.55	0.46	1236	16.65
5	1.32	0.6	0.48		
6	1.45	0.68	0.5	1386	28.83
7	1.6	0.74	0.53	1464	36.05
8	1.75	0.82	0.56	1540	63.92
9	1.92	0.9	0.58	1522	71.11
10	2.26	0.89	0.47	1258	138.68

[a] D is the mean pore size, W_t, the total specific pore volume, W_0, the specific micropore volume, S_{BET}, the BET specific surface area, and S_{EXT}, the external specific surface area.

The samples obtained by successive cyclic treatments were characterized by N_2 adsorption. The porosity of the samples was characterized by the N_2 adsorption isotherms measured using a Micromeritics ASAP 2000M at 77 K. Before the measurements, the samples were outgassed at 523 K for 24 h under a residual vacuum of less than 10^{-4} Pa. The isotherms were analyzed according to Dubinin's theory.[26,27] The mean pore size D and the specific microporous volume were estimated from the linear part of the Dubinin−Radushkevich (D−R) plot.[27,28] The S_{BET} values were estimated from the nitrogen isotherm analysis. The Sing α plot (using black carbon Vulcan 3 as reference) is used to obtain values of the external surface S_{EXT}. As the solids have low external surface areas compared to the BET surface ($S_{EXT} \ll S_{BET}$), the specific total pore volume (W_t) was estimated directly from the amount of gas adsorbed at a relative pressure of P/P_s of 0.95. The textural data are listed in Table 1.

The ^{129}Xe NMR experiments were carried out using a Bruker ASX 500 spectrometer at the basic resonance frequency of 138.34 MHz. To increase the sensitivity we used enriched xenon (∼99% ^{129}Xe) produced by the Zelenogorsk Electrochemical Plant. The recycling time and the $\pi/2$ radio frequency pulse width used in the experiments were 5 s and 14 μs, respectively. ^{129}Xe NMR spectra were referenced to the chemical shift of gaseous xenon extrapolated to zero pressure.

The samples were placed in 10-mm NMR tubes fitted with a coaxial ground-glass vacuum stopcock and treated overnight under vacuum (10^{-1} Pa) at 523 K. Xenon adsorption equilibrium was obtained after 30 min at 297 K. The corresponding amount was calculated according to the pressure difference at a constant volume. Variable temperature chemical shift measurements were performed over the range of 150−304 K for a low xenon density, $\rho = 0.5$ mmol·cm^{-3}. The xenon concentration was roughly constant with the temperature decrease since the amount of gaseous xenon in the free volume of the ampule was negligible compared to the amount adsorbed. The ampule was cooled for 30 min and equilibrated for an additional 30 min.

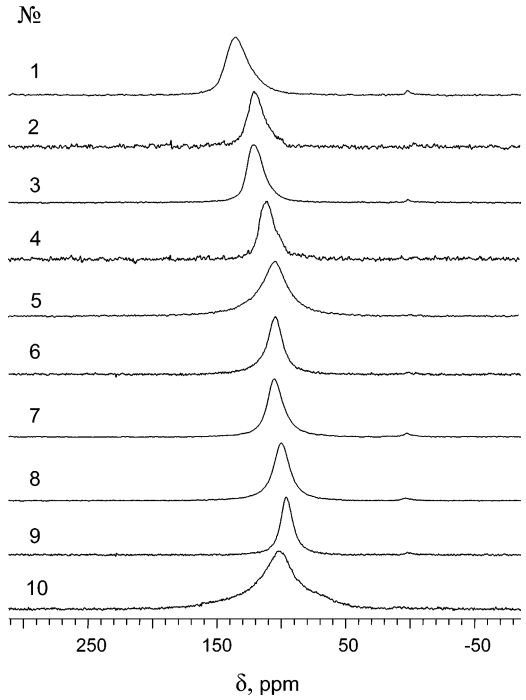

Figure 1. ^{129}Xe NMR spectra of xenon adsorbed on activated carbons (treatment cycles nos. 1−10) at a pressure ∼100 kPa.

3. Results and Discussion

The ^{129}Xe NMR spectra of xenon adsorbed on activated carbons from the same series exhibited a single line in a wide range of xenon densities (ρ). Figure 1 displays some of these spectra acquired at a xenon pressure around 100 kPa. A line-width narrowing with increasing cycle number (∼ pore size) was observed in addition to a line-shape pressure dependence (not shown). A line-width increase at increasing xenon pressure was observed for the first four treatment cycles along with the development of a small line-shape asymmetry with a tail to higher field. These features related to the chemical shift anisotropy and the pore structure heterogeneity are not easily separated by line-shape analysis. The former contribution is expected for the narrowest micropores only.[29−32] When the pore size is large enough, only the isotropic shift is observed due to effective averaging of the chemical shift tensor. The ^{129}Xe NMR spectrum of sample no. 10 was appreciably widened compared to the other samples. These changes clearly indicated some dramatic pore structure changes in the last treatment cycle.

The chemical shifts measured for the series of activated carbons as a function of xenon density ρ are illustrated in Figure 2. The density was calculated as the amount of adsorbed xenon divided by the total pore volume W_t of the sample considered (Table 1). All these plots were linear in the xenon pressure range of 0−100 kPa and could be described as

$$\delta^i = \delta^i_S + \delta^i_{Xe-Xe}\rho \quad (4)$$

where i is the treatment cycle number. Both δ^i_S and δ^i_{Xe-Xe} were calculated and compared to the corresponding pore sizes, Figures 3 and 4, respectively.

The chemical shift extrapolated to zero loading (δ_S) varied within 10 ppm over the pore size range 0.6−2.3 nm. No regular behavior of δ_S was observed. Thus, δ_S could scarcely be used as a pore size probe. Although in the case of zeolites and various molecular sieves, the variation of δ_S is not perfect either;[18] it is generally monotonic with the pore size.

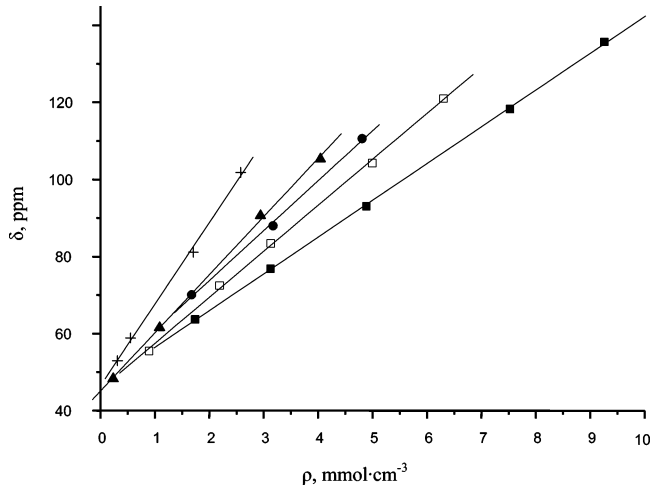

Figure 2. ^{129}Xe NMR chemical shifts vs xenon density ρ: (■) no. 1; (□) no. 3; (●) no. 4; (▲) no. 6; (+) no. 10.

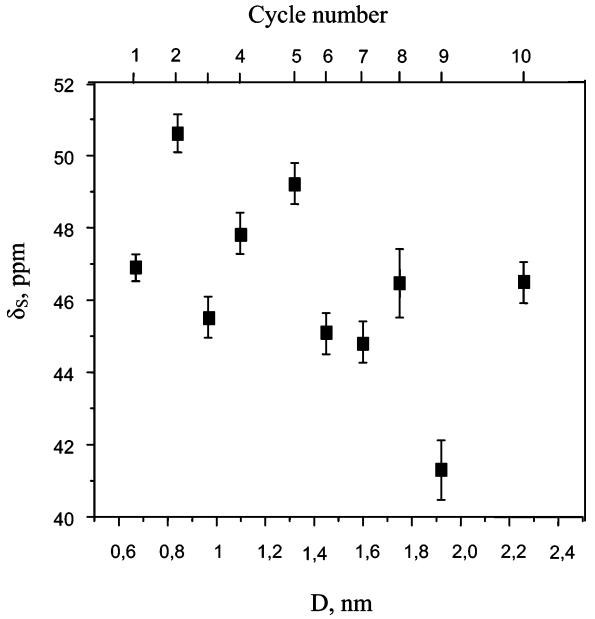

Figure 3. ^{129}Xe NMR chemical shifts approximated to zero xenon density vs mean pore size. The treatment cycle numbers are given on the upper axis.

On the contrary, the slope δ_{Xe-Xe} varied significantly and regularly with the pore size (Figure 4). We can propose a linear $\delta_{Xe-Xe}-D$ relationship to describe our experimental data:

$$\delta_{Xe-Xe} = \eta + \kappa D \quad (5)$$

where δ_{Xe-Xe} is the chemical shift slope (ppm·cm^3·mmol^{-1}), D is the mean pore size (nm), κ is 7 ± 0.2 (ppm·cm^3·mmol^{-1}·nm^{-1}), and η is 5.1 ± 0.3 (ppm·cm^3·mmol^{-1}).

Generally, $\delta_{Xe-Xe}(D)$ is proportional to the xenon collision frequency and, therefore, to the molecular collision cross-sectional area (σ). The latter is a geometrical factor, which can be calculated according to the known pore structure. Therefore, to some extent, the character of $\delta_{Xe-Xe}(D)$ reflects the pore geometry.

Though the activated carbons differ from zeolites in surface chemical properties and their micropore structure does not correspond to any ideal geometry,[33] it is interesting to compare the magnitudes of the slope δ_{Xe-Xe} obtained for a known pore

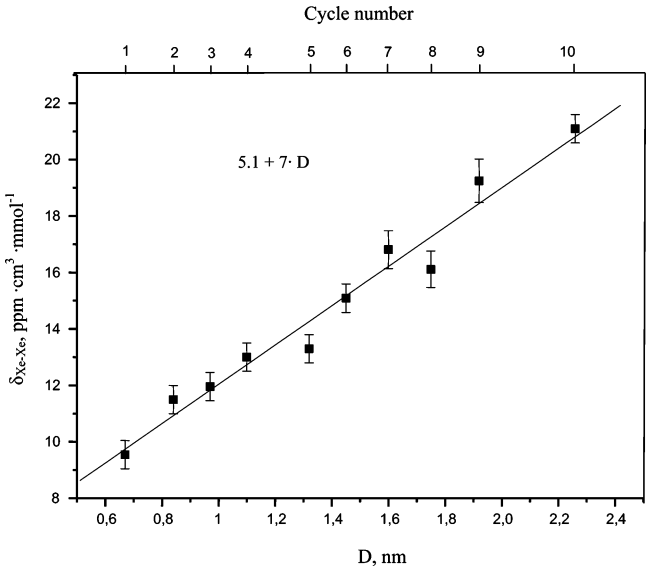

Figure 4. Experimental δ_{Xe-Xe} values vs mean pore size obtained for the series of activated carbons (■). The treatment cycle numbers are given on the upper axis. The linear fit of the experimental data $\delta_{Xe-Xe} = 5.1 + 7D$ is shown with a solid line.

structure (cylinder) and that for the unknown one of activated carbons. The term δ_{Xe-Xe} (ppm·cm^3·mmol^{-1}) can be derived using eq 3b:

$$\delta_{Xe-Xe} = 7.89D^2 \tag{6}$$

This equation is valid in the range between one and two times the xenon diameter: $D_{Xe} \leq D \leq 2D_{Xe} \sim 0.9$ nm. The pore sizes of the first three activated carbons (nos. 1−3) were within the range of validity of eq 6 (eq 3b). However, the corresponding δ_{Xe-Xe} values are considerably greater than the theoretical values deduced from eq 3. For example, a maximal value of $\delta_{Xe-Xe}(D)$ (eq 6) over the range 0.4−0.9 nm is estimated at $\delta_{Xe-Xe} = \delta_{Xe-Xe}(2D_{Xe}) \sim 6.1$ ppm·cm^3·mmol^{-1}. This is close to $\delta_{bulk}/2$, where δ_{bulk} is the value obtained for bulk xenon: $\delta_{bulk} = 0.548$ ppm·amagat^{-1} = 12.2 ppm·cm^3·mmol^{-1}.[13]

The fact that the δ_{Xe-Xe} values obtained with eq 6 are quite far from our experimental data is not surprising in view of all the simplifications made in this model. First, the diffusion of xenon in activated carbons should be regarded as a three-dimensional motion in a complex (not cylindrical) pore framework. Second, the heterogeneous structure of the pore walls is not taken into account. Although it is doubtful that the $\delta_{Xe-Xe}-D$ correlation obtained in this study could be rationalized simply in terms of the xenon collision model, the positive slope led us to propose that the xenon collision frequency increases with increasing pore size.

Since the temperature dependence of the chemical shift $\delta(T)$ is sensitive to the shape of the potential experienced by the xenon atom, it was expected to provide us with supplementary information on the pore structure and surface properties of activated carbons. Several models describing the chemical shift of xenon as a function of temperature have been developed and examined for zeolites.[34−38]

Examination of the activated carbons pore geometry could be useful by means of ^{129}Xe NMR if one could find a suitable approach. For instance, the slitlike pore geometry, often considered for activated carbons, can be examined with the model proposed by Cheung.[38] This model describes the chemical shift of a single xenon atom confined in slit,

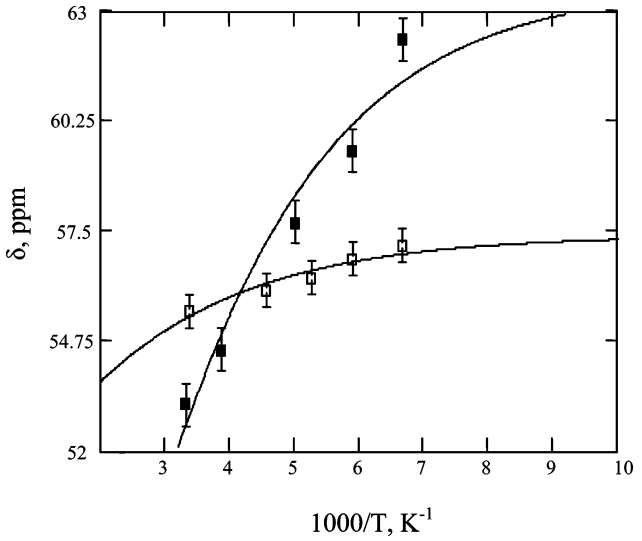

Figure 5. Chemical shifts vs reciprocal temperature measured for samples no. 1 (□) and no. 9 (■). The curves represent the least-squares fits of eq 7 to the experimental data.

cylindrical, and spherical micropores:

$$\delta(T) = \frac{C\epsilon}{1 + F\exp(-\epsilon/T)} \tag{7}$$

where $F = (L - D_{Xe})/(2lm - 1)$; L (Å) is the free pore size; D_{Xe} is the xenon diameter (4.4 Å); $m = 1$, 2, and 3 for slit, cylindrical, and spherical pore geometries, respectively; ϵ (K) and l (Å) are respectively the potential well depth and width; and C (ppm/K) is a phenomenological constant. According to Cheung's calculations, the chemical shift can be an increasing or decreasing function of temperature depending on the pore size. If the pore size is close to the xenon atom radius, the chemical shift increases with increasing temperature. However, it decreases for sufficiently large pores, i.e., $L + 2R_a > 2.6(R_{Xe} + R_a)$, where R_{Xe} and R_a are the van der Waals radii of Xe and surface atoms, respectively.

Variable temperature chemical shift measurements were performed for the sample nos. 1 and 9 at a low xenon density, $\rho = 0.5$ mmol·cm^{-3}. The xenon density was assumed to be constant and independent of temperature, since the amount of gaseous xenon in the free volume of the ampule was negligible compared to the amount adsorbed. Under these conditions, the chemical shift changed by 2 and 9 ppm over the temperature range 150−304 K for nos. 1 and 9, respectively, Figure 5. Since the coverage of the carbon surface by xenon was very low in these experiments, no xenon liquefaction should be considered (the melting point of xenon in the bulk is 163 K). Indeed, the xenon density used was equal to 3 atoms per 10 nm^3. These atoms interact with the surface much more strongly than with each other. If liquefaction or solidification of xenon occurred, additional lines downfield from the adsorbed phase would appear or the chemical shifts observed for nos. 1 and 9 at 150 K would be equal, which was not the case.

Regarding the adequacy of the model proposed by Cheung to our data, the most important issues are the pores structure heterogeneity resulting in the fitting parameters spread and the surface nature of activated carbons, which is different from zeolites. With this in mind, F and ϵ were chosen as adjustable parameters. The constant C was fixed at the value 0.127/k (ppm/K) (k is the Boltzmann constant), obtained in accordance with ref 39.

The curves displayed in Figure 5 represent the least-squares fits of eq 7 to the experimental data. The corresponding parameter values are $\epsilon_1 = 451$ K and $F_1 = 0.17$ and $\epsilon_9 = 500$ K and $F_9 = 1.1$ for no. 1 and no. 9, respectively.

Assuming free pore size values L equal to the mean pore sizes $D_1 = 6.7$ and $D_9 = 19.2$ Å (Table 1) and using the expression for F given above, one obtains $l_1m_1 = 7.4$ and $l_9m_9 = 7.3$ ($lm = (L - D_{Xe})/2F + {}^1/_2$) for samples no. 1 and no. 9, respectively. While our data do not cover a sufficient temperature range to test the validity of Cheung' model, assumptions about certain model pore geometries could be confirmed with these figures.

The slitlike pore model is to be checked first as it is a classical approach for modeling the porosity of activated carbons. In the case of no. 1, $m_1 = 1$ led to $l_1 = 7.4$ Å. Since the condition $2l_1 < D_1 = 6.7$ Å must be satisfied (the factor of 2 corresponds to the double well width distance, which fit between two adjacent pore walls), this value of the potential well width is too large for the pore size of 6.7 Å. According to the later condition, the valid value l_1 should not exceed $D_1/2 \sim 3.3$ Å. Thus, since $l_1m_1 = 7.4$ and $l_1 < 3.3$, we obtain $m_1 > 2.2$, i.e., the pores of no. 1 could not be considered to be slitlike. This conclusion is valid also for no. 9, if we assume that l remains the same for all considered materials. Finally, on the basis of Cheung's model, one could conclude that the pore structure of sample no. 1 approaches a cylindrical geometry while that of sample n*o*. 9 is closer to a spherical geometry. However, according to the study,[33] the pore morphology of carbons obtained from a unique precursor by air oxidation/pyrolysis cycles is not slitlike indeed. From those results, it was chosen to consider the edge/edge and edge/face nanomorphologies of porosity available between disklike BSU (basic structural units).

Generally, the range of the chemical shift variation with temperature increases with increasing heterogeneity of the xenon−surface interaction potential inside the pores. Indeed, the chemical shift was almost independent of the temperature for the smallest micropores $D = 0.67$ nm (no. 1). This could be ascribed to high potential homogeneity inside the micropores, when no preferential localization of xenon occurs as the temperature decreases. Our observation was similar to that reported for zeolite ZSM5, when the chemical shift varied within 6 ppm over the temperature range 173−373 K.[40] This similarity could be rationalized by the similar pore dimensions of no. 1 and ZSM5. The chemical shift regarded as a statistical average is influenced by the temperature and the pore size through the thermodynamic equilibrium ratio of the residence times of xenon on the surface and in the free space.

However, the chemical shift behavior established for activated carbons is different from zeolites if wider pores are considered. Though the temperature influence exhibited for no. 9 was more pronounced than that for no. 1, it was substantially weaker than those observed for microporous zeolites of a proximate pore size and mesoporous or amorphous silica.[40−43] For instance, a chemical shift variation of 50 ppm over the temperature range 173−373 K is reported for Y zeolite ($D = 1.3$ nm). This is much greater than the range of 9 ppm observed for no. 9 ($D = 1.92$ nm). The xenon−surface interaction potential seemed to be smoother in the latter case even for wider micropores.

4. Conclusion

Studies of porous carbon materials and especially of amorphous activated carbons are usually complicated. The results presented show that ^{129}Xe NMR data can provide very important information on the pore structure of amorphous microporous carbons. The first correlation established for the particular set of activated carbons is very promising due to its high accuracy as compared to the correlations proposed earlier for zeolites or ordered and amorphous silica. Binary xenon collisions in a confined space detected by ^{129}Xe NMR should be regarded as an effective probe of activated carbon porosity. The proposed correlation $\delta_{Xe-Xe}-D$ indicates that the xenon collision frequency increases with increasing micropore size.

Acknowledgment. The French Embassy in Moscow and the Russian Foundation of Basic Research (Grant RFBR 04-03-33070) are acknowledged for financial support. Jean-Noël Rouzaud (ENS Paris) is thanked for the initial advice which prompted this study.

References and Notes

(1) Bansal, N.; Foley, H. C.; Lafyatis, D. S.; Dybowski, C. *Catal. Today* **1992**, *14*, 305−316.
(2) Ago, H.; Tanaka, K.; Yamabe, T.; Miyoshi, T.; Takegoshi, K.; Terao, T.; Yata, S.; Hato, Y.; Nagura, S.; Ando, N. *Carbon* **1997**, *35*, 1781−1787.
(3) McGrath, K. J. *Carbon* **1999**, *37*, 1443−1448.
(4) Suh, D. J.; Park, T. J.; Ihm, S. K.; Ryoo, R. *J. Phys. Chem.* **1991**, *95*, 3767−3771.
(5) Raftery, D.; Long, H.; Meersmann, T.; Grandinetti, P. J.; Reven, L.; Pines, A. *Phys. Rev. Lett.* **1991**, *66*, 584−587.
(6) Tsiao, C.; Botto, R. E. *Energy Fuels* **1991**, *5*, 87−92.
(7) Saito, K.; Kimura, A.; Fujiwara, H. *Magn. Reson. Imaging* **2003**, *21*, 401−403.
(8) Kryukova, G. N.; Boehm, H. P.; Moroz, E. M.; Likholobov, V. A.; Filimonova, S. V.; Kuretzky, T.; Simonov, P. A. *Carbon* **1999**, *37*, 591−600.
(9) Romanenko, K. V.; d′Espinose de Lacaillerie, J.-B.; Fraissard, J.; Reshetenko, T. V.; Lapina, O. B. *Micropor. Mesopor. Mater.* **2005**, *81*, 41−48.
(10) Romanenko, K. V.; Fonseca, A.; Dumonteil, S.; B′Nagy, J.; d′Espinose de Lacaillerie, J.-B.; Lapina, O. B.; Fraissard, J. *Solid State Nucl. Magn. Reson.* **2005**, *28*, 135−141.
(11) Clewett, C. F. M.; Pietra, T. *J. Phys. Chem. B* **2005**, *109*, 17907−17912.
(12) Py, X.; Guillot, A.; Cagnon, B. *Carbon* **2003**, *41*, 1533−1543.
(13) Jameson, A. K.; Jameson, C. J.; Gutowsky, H. S. *J. Chem. Phys.* **1970,** *53*, 2310−2321.
(14) Jameson, C. J.; Jameson, A. K.; Cohen, S. M. *J. Chem. Phys.* **1973**, *59*, 4540−4546.
(15) Ito, T.; Fraissard, J. *Proc. Int. Conf. Zeolites 5th* **1980**, 510−515.
(16) Dybowski, C.; Bansal, N.; Duncan, T. M. *Annu. Rev. Phys. Chem.* **1991**, *42***,** 433−464.
(17) Demarquay, J.; Fraissard, J. *Chem. Phys. Lett.* **1987**, *136*, 314−318.
(18) Bonardet, J. L.; Fraissard, J.; Gedeon, A.; Springuel-Huet, M. A. *Catal. Rev.* **1999**, *41*, 115−225.
(19) Julbe, A.; Menorval, L. C.; Balzer, C.; David, P.; Palmeri, P.; Guizard, C. *J. Porous Mater.* **1999**, *6*, 41−54.
(20) Chen, F.; Chen, C.; Ding, S.; Yue, Y.; Ye, C.; Deng F. *Chem. Phys. Lett.* **2004**, *383*, 309−313.
(21) Kukla, V.; Kornatowski, J.; Demuth, D.; Girnus, I.; Pfeifer, H.; Rees, L. V. C.; Schunk, S.; Unger, K. K.; Kärger. J. *Science* **1996**, *272*, 702−704.
(22) Hahn, K.; Kärger, J.; Kukla, V. *Phys. Rev. Lett.* **1996**, *76*, 2762−2765.
(23) Roedenbeck, G.; Hahn, K.; Kärger, J. *Phys. Rev. E* **1997**, *55*, 5697−5712.
(24) Wei, Q.-H.; Bechinger, C.; Leiderer, P. *Science* **2000**, *287***,** 625−627.
(25) Demontis, P.; Gonzalez, J. G.; Suffritti, G. B.; Tilocca, A. *J. Am. Chem. Soc.* **2001**, *123*, 5069−5074.
(26) Bansal, R. C.; Donnet, J. B. F. *Active Carbons*; M. Dekker: New York, 1988; pp 119−162.
(27) Stoeckli, F. In *Porosity in Carbons−Characterization and Applications*; Patrick, J., Ed.; Arnold: London, 1995; pp 67−92.
(28) Stoeckli, F.; Lopez-Ramon, M. V.; Hugi-Cleary, D.; Guillot, A. *Carbon* **2001**, *39*, 1115−1116.
(29) Springuel-Huet, M. A.; Fraissard, J. *Chem. Phys. Lett.* **1989**, *154*, 299−302.
(30) Ripmeester, J. A.; Ratcliffe, C. I. *J. Phys. Chem.* **1995**, *99*, 619−622.
(31) Jameson, C. J.; Dios, A. C. *J. Chem. Phys.* **2002**, *116*, 3805−3821.

(32) Jameson, C. J. *J. Chem. Phys.* **2002**, *116*, 8912−8929.
(33) Py, X.; Guillot, A.; Cagnon, B. *Carbon* **2004**, *42*, 1743−1754.
(34) Ripmeester, J. A.; Ratcliffe, C. I. *J. Phys. Chem.* **1990**, *94*, 7652−7656.
(35) Chen, Q. J.; Fraissard, J. *J. Phys. Chem.* **1992**, *96*, 1809−1813.
(36) Jameson, C. J.; Jameson, A. K.; Gerald, R., II; de Dois, A. C. J.; Jameson, C. J.; de Dois, A. C. *J. Chem. Phys.* **1992**, *97*, 417−434.
(37) Jameson, C. J.; Jameson, A. K.; Baello, B. I.; Lim, H. M. *J. Chem. Phys.* **1994**, *100*, 5965−5976.
(38) Cheung, T. T. P. *J. Phys. Chem.* **1995**, *99*, 7089−7095.
(39) Kromhout, R. A.; Linder, B. *J. Magn. Reson.* **1969**, *1*, 450−463.
(40) Chen, Q. J.; Fraissard, J. *J. Phys. Chem.* **1992**, *96*, 1814−1819.
(41) Conner, W. C.; Weist, E. L.; Ito, T.; Fraissard, J. *J. Phys. Chem.* **1989**, *93*, 4138−4142.
(42) Terskikh, V.; Mudrakovskii, I.; Mastikhin, V. *J. Chem. Soc., Faraday Trans.* **1993**, *89*, 4239−4243.
(43) Moudrakovski, I. L.; Terskikh, V. V.; Ratcliffe, C. I.; Ripmeester, J. A.; Wang, L.-Q.; Shin, Y.; Exarhos, G. J. *J. Phys. Chem. B* **2002**, *106*, 5938−5946.